Tunable beam shaping with a phased array acousto-optic modulator

A. Grinenko,[1,*] M. P. MacDonald,[2,3] C. R. P. Courtney,[1] P. D. Wilcox,[1] C. E. M. Demore,[2] S. Cochran,[2] and B. W. Drinkwater[1]

[1] *Ultrasonics and NDT, Mechanical Engineering, University of Bristol, Bristol BS8 1TR, UK*
[2] *Division of Physics, The Institute for Medical Science and Technology, School of Medicine, University of Dundee, 1 Wurzburg Loan, Dundee DD2 1FD, UK*
[3] *mikepmacdonald@gmail.com*
[*] *alon.grinenko@gmail.com*

Abstract: We demonstrate the generation of Bessel beams using an acousto-optic array based on a liquid filled cavity surrounded by a cylindrical multi-element ultrasound transducer array. Conversion of a Gaussian laser mode into a Bessel beam with tunable order and position is shown. Also higher-order Bessel beams up to the fourth order are successfully generated with experimental results very closely matching simulations.

OCIS codes: (090.2890) Holographic optical elements; (170.1065) Acousto-optics; (230.1040) Acousto-optical devices; (090.5694) Real-time holography;

References and links

1. B. L. Ellerbroek, "First-order performance evaluation of adaptive-optics systems for atmospheric-turbulence compensation in extended-field-of-view astronomical telescopes," J. Opt. Soc. Am. **11**, 783–805 (1994).
2. D. McGloin, "Optical tweezers: 20 years on," Phil. Trans. Roy. Soc. A **364**, 3521–3537 (2006).
3. T. Cizmar, M. Mazilu, and K. Dholakia, "In situ wavefront correction and its application to micromanipulation," Nat. Photonics **4**, 388–394 (2010).
4. J. Durnin, J. J. Miceli, and J. H. Eberly, "Diffraction-free beams," Phys. Rev. Lett. **58**, 1499–1501 (1987).
5. M. Padgett and L. Allen, "The angular momentum of light: optical spanners and the rotational frequency shift," Opt. Quant. Electron. **31**, 1–12 (1999).
6. X. Tsampoula, V. Garces-Chavez, M. Comrie, D. J. Stevenson, B. Agate, C. T. A. Brown, F. Gunn-Moore, and K. Dholakia, "Femtosecond cellular transfection using a nondiffracting light beam," Appl. Phys. Lett. **91**, 053902 (2007).
7. J. Arlt, V. Garces-Chavez, W. Sibbett, and K. Dholakia, "Optical micromanipulation using a bessel light beam," Opt. Commun. **197**, 239–245 (2001).
8. L. C. Thomson and J. Courtial, "Holographic shaping of generalized self-reconstructing light beams," Opt. Commun. **281**, 1217–1221 (2008).
9. V. Garces-Chavez, D. McGloin, H. Melville, W. Sibbett, and K. Dholakia, "Simultaneous micromanipulation in multiple planes using a self-reconstructing light beam," Nature (London) **419**, 145–147 (2002).
10. J. Arlt, K. Dholakia, J. Soneson, and E. M. Wright, "Optical dipole traps and atomic waveguides based on bessel light beams," Phys. Rev. A **63**, 063602 (2001).
11. T. Wulle and S. Herminghaus, "Nonlinear optics of bessel beams," Phys. Rev. Lett. **70**, 1401–1404 (1993).
12. A. Novitsky, C.-W. Qiu, and H. Wang, "Single gradientless light beam drags particles as tractor beams," Phys. Rev. Lett. **107**, 203601 (2011).
13. J. Chen, J. Ng, Z. Lin, and C. T. Chan, "Optical pulling force," Nat. Photon. **5**, 531–534 (2011).
14. O. Brzobohaty, V. Karasek, M. Siler, L. Chvatal, T. Cizmar, and P. Zemanek, "Experimental demonstration of optical transport, sorting and self-arrangement using a /'tractor beam/'," Nat. Photonics **7**, 123–127 (2013).
15. J. Durnin, "Exact solutions for nondiffracting beams. i. the scalar theory," J. Opt. Soc. Am. **4**, 651–654 (1987).
16. J. H. McLeod, "The axicon: A new type of optical element," J. Opt. Soc. Am. **44**, 592–592 (1954).
17. G. Indebetouw, "Nondiffracting optical fields: some remarks on their analysis and synthesis," J. Opt. Soc. Am. **6**, 150–152 (1989).

#221985 - $15.00 USD Received 12 Sep 2014; revised 1 Nov 2014; accepted 3 Nov 2014; published 5 Jan 2015

18. A. J. Cox and D. C. Dibble, "Nondiffracting beam from a spatially filtered fabry-perot resonator," J. Opt. Soc. Am. **9**, 282–286 (1992).
19. A. Vasara, J. Turunen, and A. T. Friberg, "Realization of general nondiffracting beams with computer-generated holograms," J. Opt. Soc. Am. **6**, 1748–1754 (1989).
20. J. A. Davis, E. Carcole, and D. M. Cottrell, "Nondiffracting interference patterns generated with programmable spatial light modulators," Appl. Opt. **35**, 599–602 (1996).
21. E. McLeod, A. B. Hopkins, and C. B. Arnold, "Multiscale bessel beams generated by a tunable acoustic gradient index of refraction lens," Opt. Lett. **31**, 3155–3157 (2006).
22. T. Čižmár, H. I. C. Dalgarno, P. C. Ashok, F. J. Gunn-Moore, and K. Dholakia, "Optical aberration compensation in a multiplexed optical trapping system," J. Opt. **13**, 044008 (2011).
23. P. S. Hilaire, S. A. Benton, and M. Lucente, "Synthetic aperture synthetic aperture holography: a novel approach to three-dimensional displays," J. Opt. Soc. Am. **9**, 1969 (1992).
24. F. Yaras, H. Kang, and L. Onural, "State of the art in holographic displays: A survey," J. Disp. Technol. **6**, 443–454 (2010).
25. C. R. P. Courtney, B. W. Drinkwater, C. E. M. Demore, S. Cochran, A. Grinenko, and P. D. Wilcox, "Dexterous manipulation of microparticles using bessel-function acoustic pressure fields," Appl. Phys. Lett. **102**, 123508 (2013).
26. A. Grinenko, P. D. Wilcox, C. R. P. Courtney, and B. W. Drinkwater, "Proof of principle study of ultrasonic particle manipulation by a circular array device," Proc. Roy. Soc. A **468**, 3571–3586 (2012).
27. C. E. M. Demore, Z. Yang, A. Volovick, S. Cochran, M. P. MacDonald, and G. C. Spalding, "Mechanical evidence of the orbital angular momentum to energy ratio of vortex beams," Phys. Rev. Lett. **108**, 194301 (2012).
28. M. P. J. Lavery, D. J. Robertson, A. Sponselli, J. Courtial, N. K. Steinhoff, G. A. Tyler, A. E. Willner, and M. J. Padgett, "Efficient measurement of an optical orbital-angular-momentum spectrum comprising more than 50 states," New J. Phys. **15**, 013024 (2013).
29. M. Abramowitz and I. A. Stegun, *Handbook of Mathematical Functions with Formulas, Graphs, and Mathematical Tables* (Dover, 1964).
30. E. McLeod and C. B. Arnold, "Mechanics and refractive power optimization of tunable acoustic gradient lenses," J. Appl. Phys. **102**, 033104 (2007).
31. M. Born and E. Wolf, *Principles of Optics* (Cambridge University, 2003).

The capabilities of laser mode shaping and steering are crucial for optical manipulation and aberration correction applications. Depending on specific requirements of each application, these capabilities are realised using different methods which are based on establishing a certain level of control over the phase of a beam. Deformable mirrors are used for aberration corrections in astronomy [1] and spatial light modulators (SLMs) are the common choice in optical trapping applications [2] and microscopy [3]. In this letter, a novel technique is introduced in which the phase of a laser mode is modulated using a tuneable acousto-optic array. This method potentially offers very high refresh rates ($\sim$1MHz), high output power (~ 3 MW/cm^2), and is shown to be particularly well suited for generation of Bessel beams with a built-in beam steering capacity.

Non-Gaussian laser modes such as Laguerre-Gaussian and Bessel beams [4] have been used in applications as varied as the transfer of orbital angular momentum [5] and photoporation [6]. Important properties of Bessel beams such as diffraction free propagation and self-reconstructing wavefronts have driven their applications in micro-manipulation [7–9], atom optics [10] and nonlinear optics [11] while the conical wavefronts of high-order Bessel beams are being used used as tractor beams [12–14].

Although an ideal Bessel beam requires an infinitely wide wavefront to facilitate continuous propagation, approximations to Bessel beams, with a finite propagation length, have been produced by a variety of methods using bulk optical elements [15–18] and holographic techniques using computer generated static [19] and tunable holograms [20].

A method for generation of pseudo-Bessel beams using a tunable acoustic gradient lens relying on acousto-optic interaction effect has been examined in [21]. The beam tuning was achieved by controlling the magnitude of the acoustically induced refractive index gradients with the amplitude of the driving voltage. This allows the distance between the side lobes of the Bessel function of the beam to be altered, but, does not allow the Bessel beams to be steered

#221985 - $15.00 USD Received 12 Sep 2014; revised 1 Nov 2014; accepted 3 Nov 2014; published 5 Jan 2015

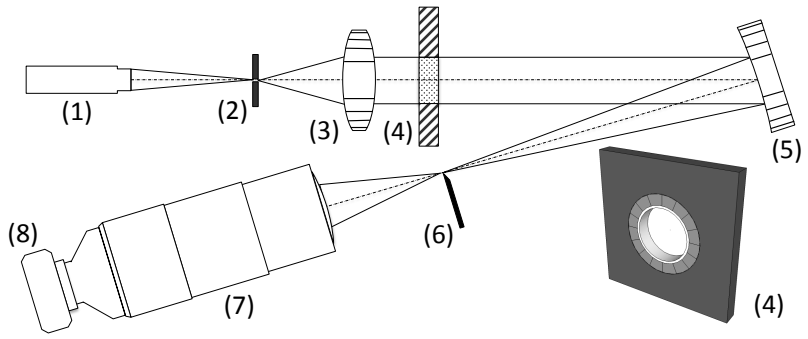

Fig. 1. Sketch of the optical setup: (1-3) laser and beam expansion system. A CPS196 adjustable focus ThorLabs 635nm diode laser (1) illuminates a $\varnothing 15\mu$m pinhole (2) located in the back focal plane of $f_3 = 10$cm lens (3); (4) the tunable acousto-optic hologram device; (5) $R_5 = 50$cm spherical mirror; (6) 0.3 mm edge; (7) AF-S NIKKOR 70-300mm zoom lens and ThorLabs KM100T CCD camera.

or higher-order beams to be generated due to the cylindrical symmetry of the device.

The SLMs on the other side allow the produced Laguerre-Gaussian and Bessel beams to be steered, however they suffer from a somewhat low refresh rate (100s of Hz), such that a combination of SLMs for creating the Bessel beams and acousto-optic deflectors for beam steering have been employed [22] due to the very fast refresh rates (several kHz) of the latter.

In general, acousto-optic devices, either of bulk or surface wave types have been widely used for a range of optical applications. Most notable in the context of the application discussed here, is their use in holographic displays where a high refresh rate is required so that the observer perceives a static image [23, 24].

Recent advances in ultrasound transducer array system allowed a sufficient degree of control over acoustic fields to be achieved [25–27] for a new type of acousto-optic device with unique tuning capabilities to be developed in which the shape of the beam and its off-axis displacement are imposed simultaneously. The potentially high ($\sim$ 1 MHz) refresh rates achievable with this method could also prove to be vital for applications such as the use of orbital angular momentum for optical signal encoding resulting in effective increase of the communication line bandwidth [28].

The system described in this letter is produced from a piezoceramic ring (PZ27) of internal radius, 5.49mm, wall thickness 0.87mm and height $d = 1.60$mm. The ring is backed with an absorbing layer (epoxy with 60% by weight alumina added) and diced into $N = 16$ elements of internal circumferential width 2.16 mm Fig. 1(4). The internal volume of the device is filled with water and is enclosed by two glass cover slips. The array was operated at a frequency of $f_a = 2.35$ MHz, an acoustic wavelength of $\lambda_a = 640$ μm, voltage amplitudes 10-25 Vpp. The choice of these parameters has been due to manufacturing convenience and could be easily adjusted for specific applications

The steering of the Bessel fields inside the fluid cavity can be accomplished by applying excitations of appropriate amplitude and phase to the piezoelectric elements [25]. An analysis of the cylindrical array carried out in [26] reveals that when an excitation consistent with the boundary conditions corresponding to Bessel field of order α is applied to the piezo-elements of the array, the resulting acoustic field consists of two contributions: the first is associated with the implied Bessel field in the central area of the device and the second is associated with Nyquist aliasing due to the finite number of the array elements. The total acoustic pressure field

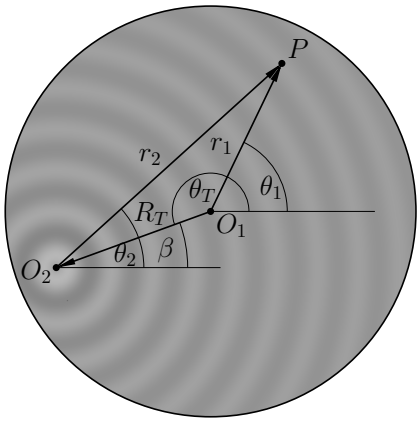

Fig. 2. Definition of coordinates systems used in Eq. (1).

generated can be shown to be of the form [26]:

$$p(x,y,t) = p_0 J_\alpha(k_a r_2) e^{i\alpha\theta_2 - i\omega_a t} + \sum_{|m|\geq M} A_m J_m(k_a r_1) e^{im\theta_1 - i\omega_a t} \tag{1}$$

where $k_a = 2\pi/\lambda_a$ is the wavenumber of the acoustic field of wavelength λ_a, ω_a is the angular frequency of the acoustic wave, (r_1, θ_1) are the polar coordinates coinciding with the centre of the array and (r_2, θ_2) are the polar coordinates coinciding with the centre of the Bessel field such that $\mathbf{r}_2 = \mathbf{r}_1 + \Delta\mathbf{r}$ and $|\Delta\mathbf{r}| = R_T$. R_T is the displacement distance of the Bessel field from the centre of the array Fig. 2 [26]. The second term in Eq. (1) corresponds to the aliasing field which is formed from a superposition of high-order Bessel functions. The lowest order of the Bessel function forming the alias is $M = N - \alpha - \pi e R_T/\lambda_a$ which, using the asymptotic behaviour of the Bessel function for large orders [29], gives the radius of the central alias-free area $r_{\min} = \lambda(N-\alpha)/\pi e - R_T$ [26]. The maximum distance to which the Bessel field can be shifted from the centre is therefore $R_{T\max} = 1/2(N-\alpha)\lambda_a/\pi e$, and the maximum order of the Bessel function that can be generated is $\alpha_{\max} = {}^1/_3 N$.

The variations in refractive index of the medium induced by this acoustic field can be imprinted on a plane electromagnetic wave propagating in the axial z direction. Consider a plane electromagnetic wave of amplitude $\mathbf{E}_0$ incident on the front optical surface $z = 0$ of the device. The field distribution at the back surface $z = d$ will be

$$E(x,y,d) = E_0 e^{ikd[n_0 + n_A(x,y,t)]} \tag{2}$$

where $k = 2\pi/\lambda$ is the wavenumber and λ is the wavelength of the optical field in the air, n_0 is the average refractive index of the filling medium and n_A is the perturbation pressure-dependant refractive index [30]. Its dependance on the pressure field is found using the Lorentz-Lorenz [31] equation

$$n_A(x,y,t) = \frac{n_0^4 + n_0^2 - 2}{6n_0} \mathbf{Re}\{\overline{p}(x,y,t)\} \tag{3}$$

where $\overline{p} \equiv p/\rho_0 c_0^2$ is the normal pressure amplitude, ρ_0 is the average mass density and c_0 is the sound velocity in the medium. Note that since the frequency of the acoustic field is much lower than that of the optical field, a fixed pressure field $p(x,y,t) = p(x,y,t_0)$ can be assumed without loss of generality for the analysis of optical fields. For excitation pressure amplitudes of

#221985 - $15.00 USD Received 12 Sep 2014; revised 1 Nov 2014; accepted 3 Nov 2014; published 5 Jan 2015

$p_a \sim 10$kPa, average density of $\rho_0 = 1$ kg/m^3, sound velocity of $c_0 = 1.5$ km/s and $n_0 = 1.33$ for room temperature water the estimated amplitude of n_A is $\sim 1.63 \times 10^{-5}$ and correspondingly $kdn_A \sim 0.025$. Thus, using a small parameter expansion the field distribution at the back plane can be written as

$$\mathbf{E}(x,y,d) = \mathbf{E}_0 e^{ikn_0 d}\left[1 + ikdn_A(x,y,t)\right]. \tag{4}$$

where the first term in the brackets is a non-diffracted plane wave and the second term corresponds to the diffracted light. The refractive power RP expressing the efficiency of power conversion from the incident plane wave into the modulated beam can be defined as $RP \equiv {}^1\!/_2 kd|\max\{n_A\}|^2$ [30]. A 0.03% efficiency is achieved for pressure amplitude of 10 kPa ($\overline{p} \sim 4.4 \times 10^{-6}$) in water-based device whereas in a solid state medium, e.g. $LiNbO_3$ with $n_0 \sim 2.286$, the same normal pressure $\overline{p}$ yields an optical efficiency of 1%. This is an upper limit of the efficiency imposed by the linearity condition of the phase modulation assumed in Eq. (4). Considering an optical surface damage threshold of ~ 300 MW/cm^2 for $LiNbO_3$ a 1% optical efficiency corresponds to a diffracted output optical power density of ~ 3 MW/cm^2. Another important parameter, the refresh rate, is determined by the the single pass-time of acoustic wave across the volume which is $\sim 7\mu$s (~ 150 kHz) in the current configuration. In a $LiNbO_3$ device of similar dimensions, the refresh rate will be 734 kHz and in a device of half the inner radius, refresh rates of 1.5 MHz would be achieved.

The propagation of the imprinted electromagnetic wave can be described using the Rayleigh-Sommerfeld integral which gives the electric field distribution at plane z behind the hologram

$$\mathbf{E}(x,y,z) = \frac{iz}{\lambda_0} \oint dx'dy' \mathbf{E}(x',y',d) \frac{e^{ik|\mathbf{r}-\mathbf{r}'|}}{|\mathbf{r}-\mathbf{r}'|} \tag{5}$$

where $|\mathbf{r}-\mathbf{r}'| = \sqrt{z^2 + (x-x')^2 + (y-y')^2}$ and the integration is performed over the area of the hologram. Substituting the acoustic field distribution Eq. (1) for $\alpha = 0$ into Eq. (5) the properties of the quasi J_0 beam propagation can be examined. The beam spreading and maximum beam intensity variation as a function of propagation distance can thus be examined and its non-diffracting properties [4, 17] established. Typically, the on-axis intensity oscillates around a fixed value until the shaped field starts to deteriorate spatially at a distance of approximately $z_{\max} = R\lambda_a/\lambda$ [4, 17]. For the array aperture radius of $R = 5.0$ mm, the acoustic wavelength of $\lambda_a = 640\mu$m and the optical wavelength of 635 nm this gives $z_{\max} \sim 5$ m.

The experimental setup is shown in Fig. 1. A $\lambda = 635$nm plane electromagnetic wave is generated by a system of a $\varnothing 15\mu$m pinhole located in the back focus of the $f_1 = 10$cm lens and adjustable focus laser (the built-in lens was used to focus the laser on the pinhole, however, this can be facilitated by a fixed mode laser and an external lens). This wave passes through the device which imprints the phase according to Eq. (4) with the refractive index $n_A(x,y)$ determined by the pressure field in the volume of the device. The strong background radiation corresponding to the first term in the brackets of Eq. (4) is removed with a high-pass spatial filter using a system of a spherical mirror of $R_5 = 50$ cm curvature radius and a 100μm wire tip placed in the focus of the mirror. The intensity profile of the resulting beam was imaged using a CCD camera and 70-300 mm zoom lens. To achieve the desired image magnification, afocal zoom system was set at 300 mm, while the position of the focusing lens had no effect on the image. This demonstrates that the Bessel is stable for at least ~ 1.5 m, which is the distance between the zoom lens and the acousto-optic array (Fig. 1(a)).

Note, that according to Eq. (1) the Bessel beam produced rotates with the angular velocity of $\omega_a = c_0 k_a$ corresponding to the $f_a = 2.35$ MHz operating acoustic frequency. Since this frequency is much higher than the CCD camera exposure time, the intensity image observed in

#221985 - $15.00 USD Received 12 Sep 2014; revised 1 Nov 2014; accepted 3 Nov 2014; published 5 Jan 2015

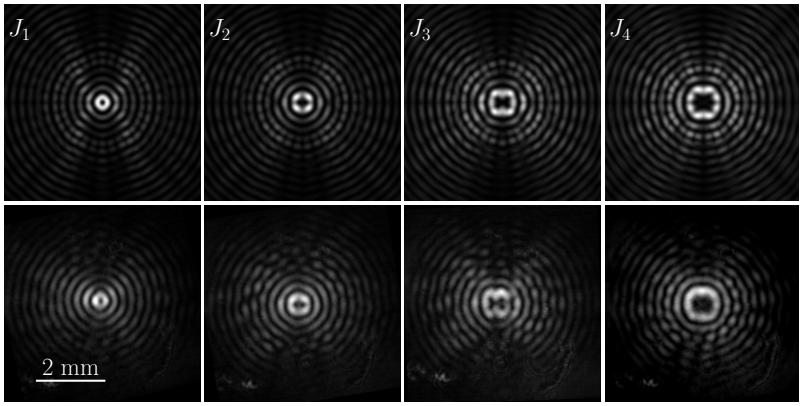

Fig. 3. intensity profiles of high-pass filtered Bessel beams of orders $\alpha = 1 \ldots 4$ produced in simulation (top) and obtained experimentally (bottom).

the CCD plane $I(X,Y)$ is in effect an angle average

$$I(X,Y) \propto \left| \frac{1}{2\pi} \int_0^{2\pi} \widetilde{n}_A(r, \theta - \Delta\theta)\, d\Delta\theta \right|^2 \tag{6}$$

where $\Delta\theta = \omega_a t$ and $\widetilde{n}_A(r,\theta)$ is the imprinted beam profile modified by the spatial high-pass filter system. Therefore, this system does not allow the instantaneous Bessel beams to be observed directly and an optical beam propagation simulation was used to assess the Bessel beams generated. The beam profiles produced in simulations assume refraction indexes to be determined by the pressure distribution given by Eq. (1). The $\tilde{n}_A$ profile is found by applying a 100μm dark field filter in Fourier space and the inverse Fourier transform is subsequently angle averaged according to Eq. (6).

Simulated and experimentally obtained cross-sections of Bessel beams of orders $\alpha = 1 \ldots 4$ are shown in Fig. 3. The good agreement between the simulated and measured beam profiles indicates that indeed higher-order Bessel beams are produced. Furthermore, the observed independence of the beam intensity image on the focal depth of the camera objective lens implies

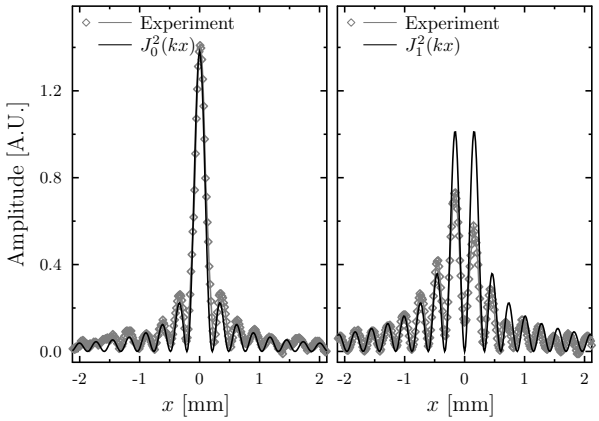

Fig. 4. Cross sections of the detected J_0 and J_1 beam intensities.

#221985 - $15.00 USD Received 12 Sep 2014; revised 1 Nov 2014; accepted 3 Nov 2014; published 5 Jan 2015

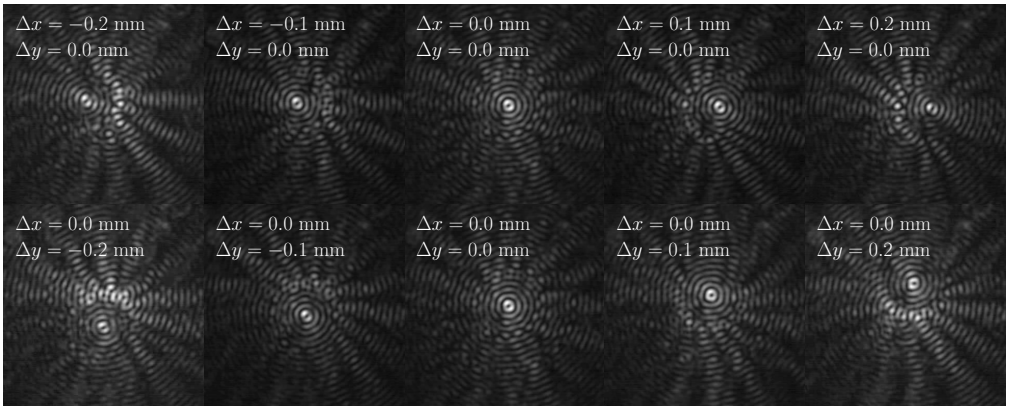

Fig. 5. The profiles of the J_1 Bessel beam manipulated in two transverse directions.

that the beam propagates a distance of several meters corresponding to the focal depth of the lens. One can see that both in simulation and in experiment the average intensity images of beam profiles are not azimuthally symmetric. The source of this asymmetry lies in the spatial filter used not being rotationally symmetric. Beam intensity profiles presented in Fig. 4 show the J_0 and J_1 beam intensities along the $Y = 0$ axis in the CCD image plane. An excellent agreement with the J_0 and J_1 functions can be seen. The better quality of the J_0 beam can be attributed to the fact that J_0 beam does not rotate like the higher-order beams and therefore it is less susceptible to the distortion introduced by the asymmetric spatial filter.

Higher-order Bessel fields produced are shown in Fig. 3 and here some of their fundamental features can be examined. The typical distortion surrounding the central area of the pure Bessel mode and its dependence on the order α of the Bessel mode implied by Eq. (1) can be seen. Thus, for $\alpha = 1$ there are four and for $\alpha = 4$ there are only two distortion free fringes implying that the size of a useful beam decreases as a function of α. It is also interesting to note that the distortion field surrounding the central area of the array produces optical field propagating in an orderly manner without disturbing the Bessel beam in the central area. The reason for this lies in the fact that the acoustic distortion field itself produces a linear superposition of Bessel beams of higher orders the lowest of which is $N - \alpha$.

The beam steering capability of the tunable acousto-optical system is demonstrated in the series of images show in Fig. 5. Here, applying corresponding phase differences to the piezo-elements of the array [25], the position of the centre of the acoustic Bessel field can be controlled within the $1/2(N-\alpha)\lambda_a/\pi e$ radius [26]. In this case a linear displacement of the beam of ± 0.2 mm in x and y directions is demonstrated.

Conclusion

A novel tuneable acousto-optic holography system has been demonstrated by the generation of optical Bessel beams of any order α below the $^1/_3N$ limit. In addition to beam generation, the system allows mechanically unaided steering of the Bessel beams produced. The physical limit on the switching rate of the system described in this letter is approximately 150 kHz but this, and the device efficiency, could be increased substantially by exciting the acoustic grating in a solid state medium such as $LiNbO_3$. It is also worth noting here that although the Bessel field distribution is intrinsic to the cylindrical arrangement of the acoustic array used in this system, the approach in principle allows to imprint any phase distribution on the optical field.

#221985 - $15.00 USD Received 12 Sep 2014; revised 1 Nov 2014; accepted 3 Nov 2014; published 5 Jan 2015